Reduced Critical Current Spread in Planar MgB_2 Josephson Junction Array Made by Focused Helium Ion Beam

Leila Kasaei, *Student Member, IEEE*, Thomas Melbourne, Mengjun Li, Viacheslav Manichev, Fei Qin, Hussein Hijazi, Leonard C. Feldman, Torgny Gustafsson, Bruce A. Davidson, XiaoXing Xi, and Ke Chen

(Invited Paper)

***Abstract*—We have fabricated series arrays of closely spaced planar Josephson junctions on MgB_2 films using a 30 keV focused helium ion beam. Uniformity of junction parameters within the arrays is sufficient for achieving phase-lock into an applied microwave signal, and flat giant Shapiro steps are observed. The spread in critical current of a 60-Josephson junction array is estimated to be less than 3.5%, significantly better than reported in MgB_2 junctions fabricated by other techniques. These results demonstrate the potential of the focused He^+ ion beam irradiation technique in MgB_2 Josephson multi-junction circuit applications such as quantum voltage standards.**

***Index Terms*—Focused helium ion microscope (HIM), Josephson junction and series array, lumped array, MgB_2, voltage metrology.**

I. Introduction

JOSEPHSON junctions (JJs) are the basic building blocks of superconducting electronics. A reliable and reproducible technique to fabricate junctions is necessary for scaling up superconducting circuits. One application of the Josephson effect is in electrical metrology. A conventional Josephson voltage standard (JVS) has been a better alternative to a Weston cell with improved accuracy of dc voltage measurement. The primary reason is that the Josephson voltage depends only on the frequency which can be obtained from the atomic clock (known with better than 1.7×10^{-16} uncertainty) [1]. Currently, the programmable Josephson voltage standard (PJVS) is widely used for dc and ac voltage calibration [2]. The pulse-driven ac Josephson voltage standard (ACJVS) is used for audio frequency applications and low voltage applications as quantum voltage noise source (QVNS) for noise thermometry [3]. These devices all require series arrays consisting of thousands of identical JJs with sufficiently low parameter spreads of the junctions, i.e., critical current, and normal resistance. It is also beneficial to develop lumped-element arrays instead of distributed arrays. In a lumped-element array, all of the junctions are placed in less than one-quarter of the wavelength of the RF drive frequency so that the phase of the junctions is synchronized by the applied RF signal leading to a higher voltage for a given microwave. This sets a stringent limit for the spacing between adjacent junctions in the array. For instance, a drive frequency of 16 GHz and 13500 series junctions requires a 120 nm spacing [4]. Moreover, heat generated in the stacked JJ array is difficult to be dissipated compared to a planar configuration, which allows the heat to be readily transferred to the substrate [5]. The quality of the Nb-based JJ array is excellent, fabrication of 1000 Nb/Al-AlO_x/Nb JJs for very large scale integration (VLSI) has been reported with the I_c spread from 0.8% to 8% for JJs with sizes from 1500 nm down to 200 nm [6]. Besides, the I_c spread of less than 1.6% was obtained for a series array of 200 NbTiN/Al-AlN_x/NbTiN Josephson tunnel junctions [7]. However, the transition temperature of Nb at 9.25 K or NbTiN at 14.2 K requires the device to operate at 4.2 K or < 10 K. Magnesium diboride (MgB_2), a simple binary compound with a critical temperature ∼40 K, superconducting energy gaps greater than 2 meV, and a relatively long coherence length (∼5 nm) has attracted considerable interest as an alternative to Nb-based devices that can operate at ∼20 K, where cheaper, more efficient and reliable cryocooling technology is available.

Besides specific applications, junction series arrays are a useful tool for measuring the parameter spread of Josephson junctions. The current state of the art Nb junction technology contains over 65,000 junctions [8], [9], impossible to measure individually to determine the junction parameter spread. The parameter spread obtained from measuring series arrays permits a quick evaluation, which can facilitate the further improvement of the junction production.

Ion-damaged planar Josephson junctions have been used as a promising approach in manufacturing superconducting circuits. Neon ion beam irradiated arrays of junctions have been reported on YBCO [10] and MgB_2 [11]. There are also reports on using oxygen ions to produce arrays [12], superconducting quantum

Manuscript received October 31, 2018; accepted February 22, 2019. Date of publication March 6, 2019; date of current version May 1, 2019. This material is based upon work supported by the National Science Foundation under Grant DMR–1310087. *(Corresponding author: Leila Kasaei.)*

L. Kasaei, T. Melbourne, F. Qin, B. A. Davidson, X. X. Xi, and K. Chen are with the Physics Department, Temple University, Philadelphia, PA 19122 USA (e-mail: leila.kasaei@temple.edu).

M. Li and V. Manichev are with the Department of Chemistry and Chemical Biology, Rutgers University, Piscataway, NJ 08854 USA.

H. Hijazi, L. C. Feldman, and T. Gustafsson, are with the Department of Physics and Astronomy, Rutgers University, Piscataway, NJ 08854 USA.

Color versions of one or more of the figures in this paper are available online at http://ieeexplore.ieee.org.

Digital Object Identifier 10.1109/TASC.2019.2903418

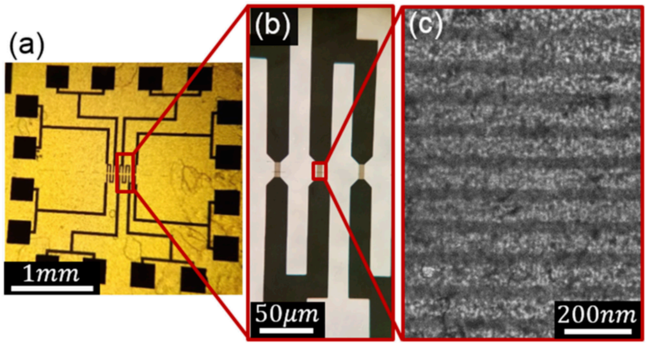

Fig. 1. (a) Optical image of the array pattern. Large bonding pads attached to a centered meandering microstrip. (b) Three branches of the meander are enlarged. Dark color lines are Au covered MgB_2. The tapered down bridges are SiO_2 covered MgB_2. (c) Zoomed view of single tracks of He^+ irradiation at 100 nm inter-spacing on a 5 μm × 15 μm bridge imaged in HIM.

interference devices (SQUIDs) [13], and superconducting quantum interference filters (SQIFs) [14] on YBCO. In recent years, focused helium ion beam irradiation attracted a lot of attention.

He^+ ion microscope (HIM) is based on a gas-field ion source (GFIS) with an ultra-sharp tip enabling the emission of an energetic beam stream of the gas ions with the diameter of less than 0.5 nm. The beam can introduce disorders into the superconducting film and suppress the critical temperature of the irradiated part, forming a barrier for a Josephson junction. This method has been well established and successfully implemented to fabricate YBCO [15], [16] and MgB_2 [17] Josephson junctions.

In this paper, we present the results of series arrays of planar MgB_2 Josephson junctions fabricated by the focused helium ion beam. With the inter-junction spacing of 100 nm, a 60-JJ array showed the spread of critical current less than 3.5%, with operating temperature up to 28 K. The result is a substantial improvement in the parameter spread in MgB_2 Josephson junctions fabricated by all techniques.

II. Experimental

Single JJ and series JJ arrays were fabricated using 25 nm thick MgB_2 thin films grown by hybrid physical-chemical vapor deposition (HPCVD) on SiC substrates [18]. To protect the surface of the MgB_2 thin film from degradation during the fabrication, a bilayer of Cr/Au (5 nm/20 nm) was deposited by DC magnetron sputtering on top of the film. Electrical bonding pads which are connected to a meandering microstrip line containing 15 μm × 5 μm bridges were patterned by standard UV lithography and argon ion milling (see Fig. 1). A second lithography and ion milling were carried out to remove the Cr/Au bilayer on top of the bridges. A 4 nm SiO_2 thin film was then deposited on the entire sample by RF magnetron sputtering for protection against the moisture. The sample was then loaded *ex-situ* into the chamber of a Zeiss Orion plus helium ion microscope. A single pixel line of 30 keV beam (the highest energy commonly available with the system with nominal beam diameter < 0.5 nm and pitch $= 1$ nm) was used to directly write Josephson junctions into the plane of the thin film at room temperature. TRIM (transport of ions in matter) software program [19] was used to simulate the He^+ ion beam interaction with the target material. The total

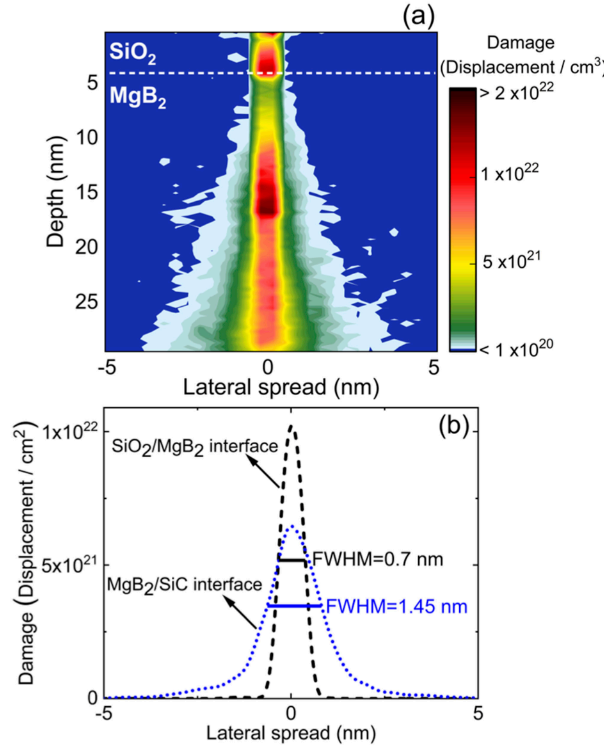

Fig. 2. (a) TRIM simulation of damage density in SiO_2/MgB_2 (4 + 25 nm) film deposited on SiC substrate when irradiated with 2.7×10^{16} ions/cm^2 He^+ ions. (b) Black dashed line represents damage profile at SiO_2/MgB_2 interface. Blue dotted line represents damage profile at MgB_2/SiC interface.

thickness of the $MgB_2 + SiO_2$ protection layer (25 nm + 4 nm) was chosen to be substantially smaller than the projected range (PR) of the 30 keV He^+ ions in the target (>150 nm). In fig. 2(a), damage density (displacement per volume, color scale) is shown within the sample suggesting that at displacement level $\sim 1 \times 10^{20}$/cm^3, the width of the damaged region, is $\sim$7.5 nm at the MgB_2/SiC interface and $\sim$1 nm at SiO_2/MgB_2 interface. This lateral spread allows for observing the Josephson effect in the MgB_2 planar junctions. Fig. 2(b) shows the damage profile for the top and bottom interfaces of MgB_2 film, indicating that the lateral spread of the damage characterized by the full width at half maximum (FWHM) is nearly doubled by the time ions reach the bottom of the film.

Our previous study on the irradiation effects in MgB_2 showed that increasing focused He^+ ion beam irradiation, induces a gradual increase in resistivity and a gradual decrease in critical temperature of the damaged region [20]. When a dose of 8×10^{15} ions/cm^2 is delivered to a large area, the material becomes normal at $T > 4$ K and dose of 2×10^{16} ions/cm^2 produces a barrier for Josephson coupling across the damaged region [17].

Single JJs and nine series arrays with the various number (10, 30, 50, 60) of JJs were written on different bridges using single pixel lines of He^+ beam with a dose of 2.7×10^{16} ions/cm^2 and 100 nm inter-junction spacing (Fig. 1(c)). Here we discuss the results on 50- and 60-JJ arrays typical of the whole set. We also present the result of a single JJ for comparison purposes.

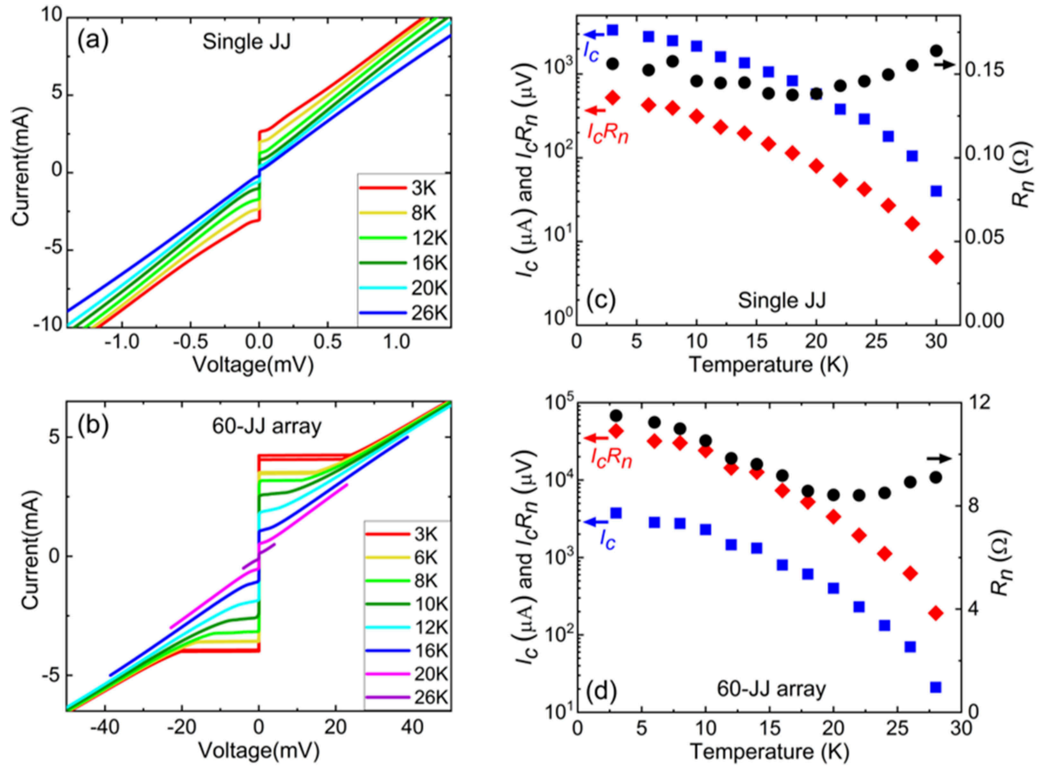

Fig. 3. Current-voltage characteristics at different temperatures for (a) single JJ, (b) 60-JJ array. Temperature dependence of the junction normal resistance (black circles), critical current (blue squares) and critical voltage (red diamonds) for (c) single JJ, (d) 60-JJ array. Compared to the single junction, normal resistance of the arrays scales with the number of junctions in the array.

III. Results and Discussion

Fig. 3(a) and 3(b) show *I–V* curves at different temperatures for the single JJ and the 60-JJ array, respectively. The fitted values of critical current (I_c), normal resistance (R_n), and characteristic voltage $(I_c R_\mathrm{n})$ to the resistively shunted junction (RSJ) model are plotted as a function of temperature in the Fig. 3(c) and 3(d). While the single JJ remained hysteresis-free down to the lowest measurement temperature of 3 K, the 60-JJ array became hysteretic at approximately 6 K. We barely observed any multiple steps around I_c of the array, which suggests minimal variations in the junction critical current in the array. For both the single JJ and the array data, the increase of the resistance with the increase in temperature and bias current indicates that the boundaries between the superconducting electrodes and the junction barrier move as temperature changes and the bias current varies, respectively, in agreement with the previous ion-damaged junction study [21]. The shape of the hysteretic *I–V* shown in Fig. 3(b) at low temperature is consistent with an SNS junction with high current density driven into non-equilibrium [22]. A couple of junctions could be hysteretic causing the hysteresis in a series array of Josephson junctions. There is a nearly constant critical current independent of the number of junctions (*N*) and an almost linear increase of R_n with *N*; subsequently, the $I_c R_n$ product also increases linearly with *N* (see Table I). While the normal resistance at 12 K for single JJ was 0.15 Ω, it roses to ∼7.8 Ω for the 50-JJ array and ∼9.8 Ω for the 60-JJ array, indicating good scaling with the single junction normal resistance. The value of $I_c R_n$ product for the 60-JJ array at 12 K was ∼14.4 mV.

TABLE I
Dependence of R_n And $I_c R_n$ on The Number of Junctions

Number of Junctions (*N*)	1	50	60
R_n (Ω) at 12 K	0.15	7.8	9.8
$\frac{R_n\,(\Omega)}{N}$	0.15	0.16	0.16
$I_c R_n$ (mV) at 12 K	0.23	13.3	14.4
$\frac{I_c R_n\,(\mathrm{mV})}{N}$	0.23	0.26	0.24

To verify that the arrays consist of Josephson junctions and assess their uniformity, the single JJ and arrays were exposed to RF radiation using an antenna placed above the chip. *I–V* characteristics were observed while adjusting microwave power and frequency. Fig. 4(a) shows current-voltage characteristics of a single JJ with different applied microwave power at frequency 11.79 GHz, measured at 24 K. Fig. 4(b) and 4(c) show giant Shapiro steps in the *I–V* curve of the 50-JJ array and 60-JJ array when applying 11.76 GHz (at 24 K) and 12.35 GHz (at 24 K) RF radiation respectively. The Shapiro steps are expected to appear at voltages: $V_n = Nn\Phi_0 f$, where *n* is an integer representing the Shapiro step index and *f* is the frequency of the RF radiation, and Φ_0 is the flux quantum. *N* will be replaced by the number of JJs in the array or 1 in single JJ. The measurements of the first voltage

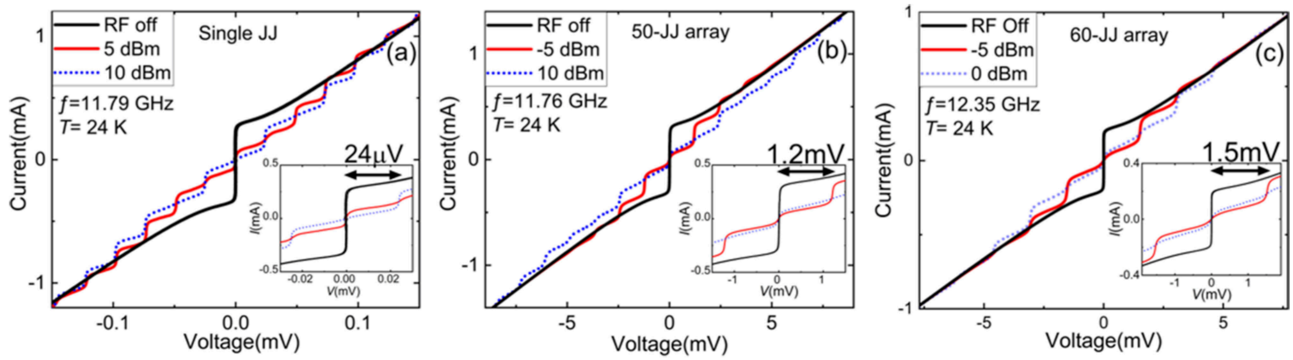

Fig. 4. Current-voltage characteristics at $T = 24$ K for (a) single junction without and with microwave radiation of $f = 11.79$ GHz at different input power levels. (b) 50-JJ series array without and with microwave radiation of $f = 11.76$ GHz at different input power levels. The space between adjacent steps in voltage is 50 times of that for an individual junction. (c) 60-JJ series array without and with microwave radiation of $f = 12.35$ GHz at different input power levels. The space between adjacent steps in voltage is 60 times of that for an individual junction.

step for single JJ (24.0 μV $\pm$ 0.1 μV), 50 JJA (1200 μV $\pm$ 4 μV), and 60 JJA (1500 μV $\pm$ 4 μV) agree with the expected voltages within the uncertainty of the measurement system. In consequence, it is evident that all the junctions are on the first step at the same time and that the junctions are tending to phase-lock to the RF current. The current amplitude of the 1st Shapiro steps (step width) in the arrays was about 0.15 mA. By reaching a large step amplitude, the array would be less susceptible to noise-induced transitions between the quantized voltage states [3].

To examine the lateral homogeneity of the barriers, the critical current of the JJ is modulated by an applied magnetic field normal to the sample surface. In the case of a single JJ, a Fraunhofer pattern which is basically the modulus of the Fourier transform of a constant critical current density within the junction is expected. In the planar geometry, the field inside the junction is much larger than the applied field due to the flux focusing effects [23] of the electrodes. Based on Rosenthal's equation, we expect the first minima in Fraunhofer pattern to occur at $\sim \pm$ 0.15 mT which agrees with the experimental result of $\sim \pm$ 0.11 mT as shown in Fig. 5(a). On the other hand, Fig. 5(b) and 5(c) illustrate the oscillatory behavior of critical current in the presence of magnetic field for 50- and 60-JJ arrays, respectively, which clearly deviates from the Fraunhofer pattern in that a plateau is formed at the field around zero. The plateau suggests some magnetic field screening, possibly resulting from close inter-junction spacing of 100 nm, comparable to the London penetration depth of MgB_2 ($\sim$100 nm at the measurement temperature [24]), since no plateau and similar to single JJ Fraunhofer pattern was observed for a 10-JJ array with 1 μm inter-junction spacing [25]. The observed interference patterns in our 50- and 60-JJ array also differ from 50 series array of YBCO step-edge junction for which Fraunhofer minima occurred at the field similar to a single junction (with no peak broadening) [26]. The comparison suggests that the ratio of inter-junction spacing to penetration depth plays an important role in the interference pattern. Further research is required to understand this phenomenon.

Additional differential resistance calculations were performed at 12 K to reveal the distribution of the individual critical currents in 50- and 60-JJ array. *I–V* curves exhibit RSJ-like behavior as low as 12 K while thermal smearing remains minimal. To evaluate the spread of the critical current in the 50- and 60-JJ arrays, we fit the experimental *dV/dI–I* curves obtained by numerical differentiation of *I–V* curves with calculated curves obtained by assuming a random Gaussian-type critical current distribution with a standard deviation σ, i.e., the I_c spread, in a series array consisting of JJs following the RSJ model at $T = 0$, namely $V(I) = R_n\sqrt{I^2 - I_c^2}$ [27]. The normal resistance R_n was assumed to be constant for each junction to follow empirical observation. Thermal smearing effect is ignored to simplify calculations and will be analyzed separately. The fitting results in Fig. 6 show overall agreement between the experimental results and the simple theoretical model except for double peaks in both 50- and 60-JJ array. The fitting parameter σ for the

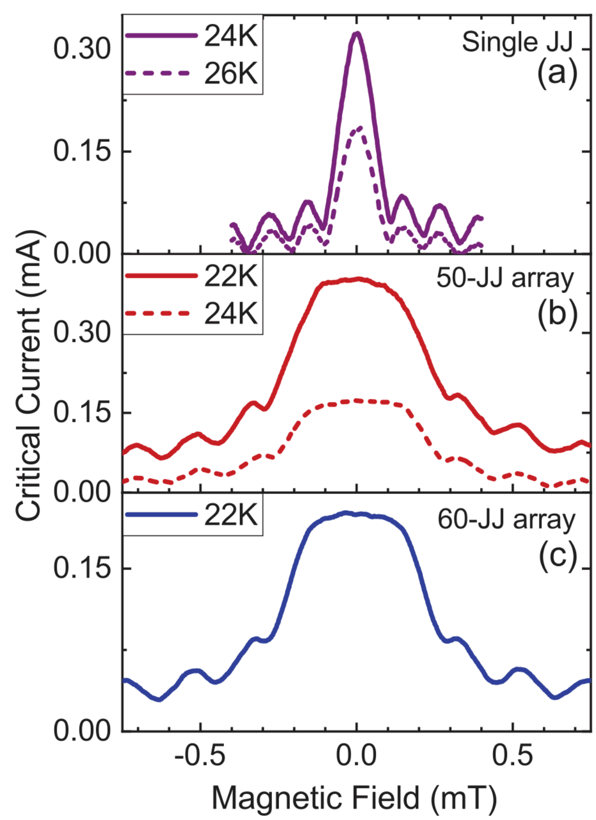

Fig. 5. Dependence of critical Josephson current on an applied magnetic field at different temperature for (a) single JJ, (b) 50-JJ array, (c) 60-JJ array.

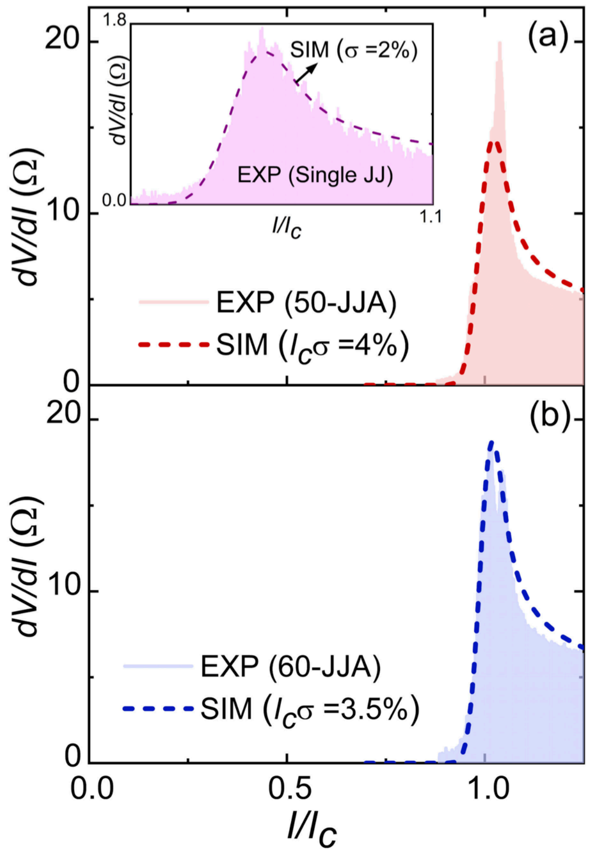

Fig. 6. *dV/dI* versus normalized current for (a) 50-, (b) 60-JJ array at $T = 12$ K. The inset shows *dV/dI* versus normalized current for single junction. Dashed lines show the simulated curves with I_c spread $\sigma = 4\%$ (50-JJ array) and $\sigma = 3.5\%$ (60-JJ array). For single JJ, the fitting parameter is 2%. Note that the simulated curves were generated by differentiating $V(I) = R_n\sqrt{I^2 - I_c^2}$ at limiting case $T = 0$ so the reported I_c spread for arrays can be considered an upper limit.

fitting is 4% and 3.5% for the 50- and 60-JJ arrays, respectively. Applying the same fitting method to a single JJ yields $\sigma = 2\%$ which can be explained by thermal smearing that was ignored in the theoretical model. Subtracting the thermal smearing, from the given spreads for arrays would result in yet lower fabrication spread. The origin of the double peak in *dV/dI* curves is not determined yet. It should be noted that HIM was ran at reduced beam current, so to reach a certain dose (2.7×10^{16} ions/cm^2) the irradiation time was extended (up to ~20 minutes for 60 JJA) which might have caused slight variation in the beam characteristic contributing to double peak features. To the best of our knowledge, the lowest reported value on the critical current spread was for a 100-JJ array of MgB_2/MgO/MgB_2 tri-layer junctions showing 54% on-chip spread of critical current [28]. Our result corresponds to less than 3.5% spread for 60-JJ array indicating a homogeneous barrier over the larger length scale which is a significant improvement over prior attempts.

IV. Conclusion

In this paper, we report the results of series arrays of densely packed planar MgB_2 Josephson junctions fabricated by direct writing using a focused helium ion beam. The 60-JJ array showed excellent uniformity and reproducibility, with a spread of the array's critical currents being less than 3.5%, indicating excellent lateral homogeneity of the barrier. The normal resistance of the array scaled proportionally to the number of junctions in the array. In addition, I_c modulation of the arrays upon applying the magnetic field showed a plateau region at the center peak which needs further study. We speculate that dc SQUID magnetometers using closely spaced arrays in two arms can benefit from their properties of high I_cR_n product, high R_n, and less suppressed critical current under the magnetic field, resulting in higher dynamic range, slew rate, and sensitivity than traditional dc SQUIDs formed by two single JJs. The results also pave the way for many other applications requiring tens to hundreds of MgB_2 Josephson junctions, such as voltage standard, quantum voltage noise source, and superconducting digital circuits, with operating temperatures above 20 K.

Acknowledgment

L. Kasaei acknowledges the use of services and facilities of Temple Materials Institute at Temple University.

References

[1] S. P. Benz, P. D. Dresselhaus, Y. Chong, and C. J. Burroughs, "Stacked nanoscale Josephson junction arrays for high-performance voltage standards," presented at the Nano and Microsyst. Technol. Metrology Conf., Arsenal, AL, USA, 2002.

[2] H. Schulze, R. Behr, J. Kohlmann, F. Müller, and J. Niemeyer, "Design and fabrication of 10 V SINIS Josephson arrays for programmable voltage standards," *Supercond. Sci. Technol.*, vol. 13, no. 9, pp. 1293–1295, Sep. 2000.

[3] S. P. Benz and C. A. Hamilton, "Application of the Josephson effect to voltage metrology," in *Proc. IEEE*, vol. 92, no. 10, pp. 1617–1629, Oct. 2004.

[4] S. P. Benz, P. D. Dresselhaus, and C. J. Burroughs, "Nanotechnology for next generation Josephson voltage standards," *IEEE Trans. Instrum. Meas.*, vol. 50, no. 6, pp. 1513–1518, Dec. 2001.

[5] Y. Chong, P. D. Dresselhaus, and S. P. Benz, "Thermal transport in stacked superconductor–normal metal–superconductor Josephson junctions," *Appl. Phys. Lett.*, vol. 83, no. 9, pp. 1794–1796, Sep. 2003.

[6] S. K. Tolpygo, V. Bolkhovsky, T. J. Weir, L. M. Johnson, M. A. Gouker, and W. D. Oliver, "Fabrication process and properties of fully-planarized deep-submicron Nb/Al–AlO_x/Nb Josephson junctions for VLSI circuits," *IEEE Trans. Appl. Supercond.*, vol. 25, no. 3, Jun. 2015, pp. 1–12, Art. no. 1101312.

[7] H. Akaike, S. Sakamoto, K. Munemoto, and A. Fujimaki, "Fabrication of NbTiN/Al–AlN_x/NbTiN Josephson junctions for superconducting circuits operating around 10 K," *IEEE Trans. Appl. Supercond.*, vol. 26, no. 5, Aug. 2016, Art. no. 1100805.

[8] S. Nagasawa *et al.*, "Nb 9-layer fabrication process for superconducting large-scale SFQ circuits and its process evaluation," *IEICE Trans. Electron.*, vol. 97, no. 3, pp. 132–140, Mar. 2014.

[9] Q. P. Herr *et al.*, "Reproducible operating margins on a 72 800-device digital superconducting chip," *Supercond. Sci. Technol.*, vol. 28, no. 12, Oct. 2015, Art. no. 124003.

[10] K. Chen, S. A. Cybart, and R. Dynes, "Study of closely spaced $YBa_2Cu_3O_{7-\delta}$ Josephson junction pairs," *IEEE Trans. Appl. Supercond.*, vol. 15, no. 2, pp. 149–152, Jun. 2005.

[11] S. A. Cybart, K. Chen, Y. Cui, Q. Li, X. X. Xi, and R. Dynes, "Planar MgB_2 Josephson junctions and series arrays via nanolithography and ion damage," *Appl. Phys. Lett.*, vol. 88, no. 1, Jan. 2006, Art. no. 012509.

[12] A. Sharafiev *et al.*, "HTS Josephson junctions arrays for high-frequency mixing," *Supercond. Sci. Technol.*, vol. 31, no. 3, Jan. 2018, Art. no. 035003.

[13] N. Bergeal, J. Lesueur, G. Faini, M. Aprili, and J. Contour, "High T_c superconducting quantum interference devices made by ion irradiation," *Appl. Phys. Lett.*, vol. 89, no. 11, Sep. 2006, Art. no. 112515.

[14] S. Ouanani *et al.*, "High-T_c superconducting quantum interference filters (SQIFs) made by ion irradiation," *Supercond. Sci. Technol.*, vol. 29, no. 9, Jul. 2016, Art. no. 094002.

[15] S. A. Cybart *et al.*, "Nano Josephson superconducting tunnel junctions in $YBa_2Cu_3O_{7-\delta}$ directly patterned with a focused helium ion beam," *Nat. Nanotechnol.*, vol. 10, no. 7, pp. 598–602, Jul. 2015.

[16] E. Y. Cho, Y. W. Zhou, J. Y. Cho, and S. A. Cybart, "Superconducting nano Josephson junctions patterned with a focused helium ion beam," *Appl. Phys. Lett.*, vol. 113, no. 2, Jul. 2018, Art. no. 022604.

[17] L. Kasaei *et al.*, "MgB_2 Josephson junctions produced by focused helium ion beam irradiation," *AIP Adv.*, vol. 8, no. 7, Jul. 2018, Art. no. 075020.

[18] X. X. Xi, "MgB_2 thin films," *Supercond. Sci. Technol.*, vol. 22, no. 4, 2009, Art. no. 043001.

[19] J. F. Ziegler, "SRIM: software," 2013. [Online]. Available: http://www.srim.org.

[20] L. Kasaei *et al.*, "Normal-state and superconducting properties of co-doped $BaFe_2As_2$ and MgB_2 thin films after focused helium ion beam irradiation," to be published.

[21] A. Katz, S. Woods, and R. Dynes, "Transport properties of high-T_c planar Josephson junctions fabricated by nanolithography and ion implantation," *J. Appl. Phys.*, vol. 87, no. 6, pp. 2978–2983, Mar. 2000.

[22] K. Likharev, "Superconducting weak links," *Rev. Modern Phys.*, vol. 51, no. 1, pp. 101–159, Jan. 1979.

[23] P. A. Rosenthal, M. Beasley, K. Char, M. Colclough, and G. Zaharchuk, "Flux focusing effects in planar thin-film grain-boundary Josephson junctions," *Appl. Phys. Lett.*, vol. 59, no. 26, pp. 3482–3484, Dec. 1991.

[24] D. Cunnane, C. Zhuang, K. Chen, X. X. Xi, J. Yong, and T. Lemberger, "Penetration depth of MgB_2 measured using Josephson junctions and SQUIDs," *Appl. Phys. Lett.*, vol. 102, no. 7, Feb. 2013, Art. no. 072603.

[25] T. Melbourne, "Magnesium Diboride Devices and Applications," Ph.D. dissertation, Phys. Dept., Temple Univ., Philadelphia, PA, USA, 2018.

[26] J. Du, J. Lazar, S. Lam, E. Mitchell, and C. Foley, "Fabrication and characterisation of series YBCO step-edge Josephson junction arrays," *Supercond. Sci. Technol.*, vol. 27, no. 9, Aug. 2014, Art. no. 095005.

[27] A. Barone and G. Paterno, *Physics and Applications of the Josephson Effect*. Hoboken, NJ, USA: Wiley, 1982.

[28] T. Melbourne, D. Cunnane, E. Galan, X. X. Xi, and K. Chen, "Study of MgB_2 Josephson junction arrays and sub-μm junctions," *IEEE Trans. Appl. Supercond.*, vol. 25, no. 3, Jun. 2015, Art. no. 1100604.